Perturbations and dynamics of reaction-diffusion systems with mass conservation

Masataka Kuwamura[1,*] and Yoshihisa Morita[2,†]

[1]*Graduate School of Human Development and Environment, Kobe University, Kobe 657-8501, Japan*

[2]*Department of Applied Mathematics and Informatics, Ryukoku University, Otsu 520-2194, Japan*

(Received 12 October 2014; revised manuscript received 30 March 2015; published 9 July 2015)

In some reaction-diffusion systems where the total mass of their components is conserved, solutions with initial values near a homogeneous equilibrium converge to a simple localized pattern (spike) after exhibiting Turing-like patterns near the equilibrium for appropriate diffusion coefficients. In this study, we investigate the perturbed reaction-diffusion systems of such conserved systems. We show that a reaction-diffusion model with a globally stable homogeneous equilibrium can exhibit large amplitude Turing-like patterns in the transient dynamics. Moreover, we propose a three-component model, which exhibits an alternating repetition of spatially (almost) homogeneous oscillations and large amplitude Turing-like patterns.

DOI: 10.1103/PhysRevE.92.012908 PACS number(s): 89.75.Kd, 82.40.Ck, 87.10.Ed

I. INTRODUCTION

Reaction-diffusion systems provide a theoretical framework for understanding pattern formation process in many fields of sciences, including chemistry, biology, and ecology. Recently, for understanding cell polarization related to the directional movements of cell, Refs. [1,2] proposed a conceptual model of a reaction-diffusion system:

$$\begin{aligned} u_t &= D_u u_{xx} + f(u,v) \\ v_t &= D_v v_{xx} - f(u,v) \end{aligned} \quad (0 < x < L), \tag{1.1}$$

under the periodic boundary condition with $D_v > D_u$, where u and v stand for concentrations of two internal chemicals in a cell. This system is called a reaction-diffusion system with mass conservation because

$$\int_0^L [u(x,t) + v(x,t)]dx \equiv \int_0^L [u(x,0) + v(x,0)]dx \tag{1.2}$$

holds for any (smooth) solutions. They showed that for appropriate functions f, a homogeneous equilibrium can be destabilized through the same mechanism as the diffusion-driven instability, and hence solutions with initial values near the destabilized equilibrium exhibit sinusoidal transient patterns, which we call Turing-like patterns. Moreover, by virtue of the mass conservation, the solutions eventually approach a simple localized pattern (spike) after exhibiting long transient dynamics; spatial patterns consisting of some spikes appear and the number of spikes decreases. This characteristic dynamics is regardless of the system size L when Turing-like patterns are observed [1]. In addition, a physically intuitive explanation on the instability of multispike patterns is also given by Ref. [1]. Following these results, mathematical aspects of Eq. (1.1) have been studied by Refs. [3–7]. In particular, for appropriate functions f, any solution converges to an equilibrium by virtue of a Lyapunov function, and a linearized stability analysis with a variational method reveals that every stable equilibrium must be constant or unimodal under the periodic boundary condition (see Refs. [3–5]).

Although Eq. (1.1) has a rather special form, we often encounter reaction-diffusion systems incorporating some additional terms into Eq. (1.1). For example, the Gray-Scott model,

$$\begin{aligned} u_t &= D_u u_{xx} - uv^2 + F(1-u) \\ v_t &= D_v v_{xx} + uv^2 - (F+k)v, \end{aligned}$$

can be regarded as the perturbed system of Eq. (1.1) if positive constants F and k are sufficiently small. We note that under appropriate conditions [8], the Gray-Scott model exhibits complex transient dynamics known as self-replication, which is caused by dynamical properties such as the diffusion-driven instability and the Bogdanov-Takens bifurcation [9].

In this paper, we consider a perturbed system of Eq. (1.1),

$$\begin{aligned} u_t &= D_u u_{xx} + f(u,v) + \varepsilon g(u,v) \\ v_t &= D_v v_{xx} - f(u,v) + \varepsilon h(u,v) \end{aligned} \quad (0 < x < L), \tag{1.3}$$

under the periodic boundary condition, where $\varepsilon > 0$ is sufficiently small. Notice that Eq. (1.3) no longer satisfies the mass conservation property, Eq. (1.2), in general. Moreover, we consider a three-component perturbed system of Eq. (1.1),

$$\begin{aligned} u_t &= D_u u_{xx} + f(u,v) + \varepsilon g_1(s,w) \\ v_t &= D_v v_{xx} - f(u,v) + \varepsilon g_2(s,w) \quad (0 < x < L), \\ w_t &= \varepsilon h(s,w) \end{aligned} \tag{1.4}$$

under the periodic boundary condition, where $w = w(t)$ and

$$s = s(t) := \frac{1}{L}\int_0^L (u+v)\,dx. \tag{1.5}$$

Here, we suppose that there exists a function of $H = H(s,w)$ such that

$$\frac{d}{dt}H[s(t),w(t)] \equiv 0 \tag{1.6}$$

holds for solutions of Eq. (1.4). Notice that the total mass of u and v is not conserved, whereas that of u, v, and w is conserved if $H = s + w$.

When the parameters F and k in the Grey-Scott model are sufficiently small, the model does not exhibit fascinating dynamics. In fact, the system has a simple dynamical structure if $F = k = 0$. Here, we are interested in the case that the unperturbed system Eq. (1.1) allows the Turing-like patterns

*kuwamura@main.h.kobe-u.ac.jp

†morita@rins.ryukoku.ac.jp

and the perturbed systems could exhibit a certain complex transient dynamics. The purpose of our study is to investigate the dynamics affected by perturbations to such reaction-diffusion systems with mass conservation. Specifically, applying the theory of fast-slow systems, we design curious dynamics of Eqs. (1.3) and (1.4), which have not been realized by the traditional Turing theory. As a result, a new aspect for Turing mechanism in reaction-diffusion systems is provided and it would be helpful for understanding some complex spatiotemporal patterns.

The remainder of this paper is organized as follows. In Sec. II, we provide a general framework for analyzing the onset of Turing-like patterns in the perturbed reaction-diffusion systems Eq. (1.3). Then, we show that a reaction-diffusion model with a globally stable homogeneous equilibrium can exhibit large amplitude Turing-like patterns in the transient dynamics. According to a standard stability analysis and bifurcation theory [10], in two-component reaction-diffusion systems, Turing patterns are realized by stable stationary solutions bifurcating from a homogeneous equilibrium. This implies that such a system never allows a globally stable homogeneous equilibrium. Therefore, our model provides a viewpoint for understanding the Turing mechanism that generates spatial patterns by the effect of diffusion. Recall that the Turing-like patterns we deal with are transient patterns.

In Sec. III, we propose a three-component model that exhibits an alternating repetition of spatially (almost) homogeneous oscillations and large amplitude Turing-like patterns. According to a dynamical systems theory [11], an alternating repetition of two different states is realized by the (approximate) construction of a periodic orbit by using heteroclinic connections between the different states. In contrast, our alternating repetition is induced by the destabilization of a spatially homogeneous oscillation by the diffusion, and the repetition seems to be given by a periodic orbit connecting a transient state (Turing-like pattern) and a spatially homogeneous oscillation. Concluding remarks are presented in Sec. IV.

II. PERTURBATIONS WITHIN SYSTEMS

A. Unperturbed systems

We consider a reaction-diffusion system,

$$\begin{aligned} u_t &= D_u u_{xx} + f(u,v) \\ v_t &= D_v v_{xx} - f(u,v) \end{aligned} \quad (0 < x < L), \tag{2.1}$$

under the periodic boundary condition, where f is sufficiently smooth (at least of C^2 class). It should be noted that

$$\frac{1}{L}\int_0^L [u(x,t) + v(x,t)]dx \equiv \frac{1}{L}\int_0^L [u(x,0) + v(x,0)]dx$$

holds for any (smooth) solutions of Eq. (2.1). Let (u^*,v^*) be a homogeneous equilibrium of Eq. (2.1) defined by

$$f(u^*,v^*) = 0. \tag{2.2}$$

Putting $f_u^* := f_u(u^*,v^*)$ and $f_v^* := f_v(u^*,v^*)$, we assume

$$f_v^* > f_u^*.$$

This condition implies that (u^*,v^*) is a stable equilibrium of the system of ODEs,

$$\begin{aligned} \dot{u} &= f(u,v) \\ \dot{v} &= -f(u,v), \end{aligned} \tag{2.3}$$

which is obtained from Eq. (2.1) by dropping the diffusion terms. We note that $u(t) + v(t) \equiv u(0) + v(0)$ holds for any solutions of Eq. (2.3). By this conservation, the linearized matrix of the right-hand side of Eq. (2.3) at (u^*,v^*) has zero eigenvalue. Furthermore, we assume

$$D_v > D_u.$$

This implies that the amplitude of the u-component becomes large when spatial patterns appear, as reported in Refs. [1,2].

By using a standard linear stability analysis, it is easy to see that (u^*,v^*) is a stable equilibrium of Eq. (2.1) if

$$D_v f_u^* - D_u f_v^* < 0. \tag{2.4}$$

This condition ensures that besides the simplicity of the zero eigenvalue, the remaining eigenvalues of the linearized operator of the right-hand side of Eq. (2.1) at (u^*,v^*) are negative; thus, the nonlinear stability is shown (cf. Ref. [12]). We note that zero eigenvalue always appears because of the mass conservation.

On the other hand, (u^*,v^*) is unstable if

$$D_v f_u^* - D_u f_v^* > 0, \tag{2.5}$$

and the wavenumber of unstable Fourier mode e^{ikx} satisfies

$$0 < k^2 < \frac{D_v f_u^* - D_u f_v^*}{D_u D_v},$$

where $k = 2\pi m/L$ $(m = 1,2,\cdots)$. In this case, (u^*,v^*) is destabilized by the same mechanism as the diffusion-driven instability, and a solution generated by a small perturbation into (u^*,v^*) exhibits spatial patterns approximated by sinusoidal functions near (u^*,v^*). We call these transient sinusoidal patterns Turing-like patterns. In the next stage, the amplitude of the solution on some subintervals in $[0,L]$ increases and that on other subintervals decreases. Consequently, the solution exhibits spatial patterns consisting of some spikes for an appropriate function f. By virtue of the mass conservation property of Eq. (2.1), however, the number of spikes decreases and a single stable spike eventually remains as reported in Refs. [1,2].

B. Slow manifold

We consider a perturbed system of Eq. (2.1),

$$\begin{aligned} u_t &= D_u u_{xx} + f(u,v) + \varepsilon g(u,v) \\ v_t &= D_v v_{xx} - f(u,v) + \varepsilon h(u,v) \end{aligned} \quad (0 < x < L), \tag{2.6}$$

where g and h are sufficiently smooth functions, and $\varepsilon > 0$ is sufficiently small. To understand the dynamics of Eq. (2.6), we first consider the dynamics of the system of ODEs

$$\begin{aligned} \dot{u} &= f(u,v) + \varepsilon g(u,v) \\ \dot{v} &= -f(u,v) + \varepsilon h(u,v), \end{aligned} \tag{2.7}$$

which is obtained by dropping the diffusion terms in Eq. (2.6). Since Eq. (2.7) is reduced to Eq. (2.3) as $\varepsilon \to 0$, we see that

generically, a solution of Eq. (2.7) with an initial value $(\tilde{u}_0,\tilde{v}_0)$ moves along the line defined by $u+v=\tilde{u}_0+\tilde{v}_0$ with $O(1)$ speed, and approaches a family of stable equilibria of Eq. (2.3) defined by

$$\Gamma=\{(u,v)\mid f(u,v)=0,\ f_u(u,v)<f_v(u,v)\}.$$

This dynamics is called the fast dynamics of Eq. (2.7). Once the solution reached a neighborhood of the manifold Γ, it slowly moves along Γ following the dynamics defined by

$$\dot{s}=\varepsilon\{g[u(s),v(s)]+h[u(s),v(s)]\},\quad [u(s),v(s)]\in\Gamma, \tag{2.8}$$

where $s\,[=u(s)+v(s)]$ gives a parametrization of Γ.

In general, a solution of Eq. (2.6) with an initial value $[u_0(x),v_0(x)]$ can be approximated by that of Eq. (2.7) with an initial value $(\tilde{u}_0,\tilde{v}_0)$ if $[u_0(x),v_0(x)]$ can be regarded as a small random perturbation to $(\tilde{u}_0,\tilde{v}_0)$, i.e., $[u_0(x),v_0(x)]=(\tilde{u}_0,\tilde{v}_0)+[\varepsilon_1(x),\varepsilon_2(x)]$, where $\varepsilon_1(x)$ and $\varepsilon_2(x)$ are sufficiently small perturbations. However, the approximation is only valid until the solution approaches Γ.

We now consider the dynamics of the reaction-diffusion system Eq. (2.6) around Γ. Since Γ is not a family of equilibria of Eq. (2.6), we expect that a solution with a nonhomogeneous initial value $[u_0(x),v_0(x)]$ in a small neighborhood of Γ slowly moves along Γ following the dynamics defined by

$$\dot{s}=\frac{\varepsilon}{L}\int_0^L[g(u,v)+h(u,v)]dx, \tag{2.9}$$

where

$$s=\frac{1}{L}\int_0^L(u+v)dx.$$

Moreover, we expect that the solution moving along Γ becomes unstable and exhibits Turing-like patterns if it enters into a region defined by Eq. (2.5). As numerically shown in the next subsection, Γ is a slow manifold that plays the onset of Turing-like patterns when ε is sufficiently small.

C. Global dynamics

We deal with a reaction-diffusion model obtained from Eq. (1.3) by setting $f(u,v)=-f_1(u)+v$, $g(u,v)\equiv 0$ and $h(u,v)=-h_1(v)$, i.e.,

$$\begin{aligned} u_t &= D_u u_{xx}-f_1(u)+v\\ v_t &= D_v v_{xx}+f_1(u)-v-\varepsilon h_1(v)\end{aligned}\qquad (0<x<L), \tag{2.10}$$

under the periodic boundary condition, where f_1 and h_1 are nonnegative smooth functions satisfying the following conditions:

$$\begin{aligned} f_1(u)=0 &\iff u=0,\\ h_1(v)=0 &\iff v=0.\end{aligned} \tag{2.11}$$

A typical example of $f_1(u)$ and $h_1(v)$ is given by

$$f_1(u):=\frac{u}{u^2+a}\quad\text{and}\quad h_1(v):=v^2, \tag{2.12}$$

with a constant $a>0$. By using a standard argument based on the maximum principle, it is easily shown that a solution of Eq. (2.10) with a nonnegative initial value takes nonnegative values for all x and $t>0$. Therefore, we consider the dynamics of nonnegative solutions of Eq. (2.10).

First, we investigate an equilibrium of Eq. (2.10) defined by

$$\begin{aligned} D_u u_{xx}-f_1(u)+v&=0\\ D_v v_{xx}+f_1(u)-v-\varepsilon h_1(v)&=0\end{aligned}\qquad (0<x<L), \tag{2.13}$$

under the periodic boundary condition. Adding the first and second equations of Eq. (2.13) and integrating over $[0,L]$, we have

$$\int_0^L h_1(v)dx=0,$$

which implies $v\equiv 0$ by $h_1(v)=0$ and the second condition of Eq. (2.11). Therefore, it follows from the second equation of Eq. (2.13) that $f_1(u)=0$, which implies $u\equiv 0$ by the first condition of Eq. (2.11). Thus, Eq. (2.10) has a unique equilibrium $(u,v)\equiv(0,0)$.

Next, we investigate the global stability of the trivial equilibrium $(0,0)$. Invoking $D_v>D_u$, we define

$$\mathcal{L}(u,v):=\int_0^L\frac{D_u}{2}u_x^2+F_1(u)+\frac{D_u}{2D_v}u^2+\frac{(D_u u+D_v v)^2}{2D_v(D_v-D_u)}\,dx,$$

where $F_1(u):=\int_0^u f_1(u)du$. For any nonnegative solution $[u(x,t),v(x,t)]$, we have

$$\begin{aligned}\frac{d}{dt}\mathcal{L}[u(\cdot,t),v(\cdot,t)]&=\int_0^L D_u u_x u_{xt}+f_1(u)u_t+\frac{D_u}{D_v}uu_t+\frac{(D_u u+D_v v)}{D_v(D_v-D_u)}(D_u u_t+D_v v_t)\,dx\\ &=\int_0^L[-D_u u_{xx}+f_1(u)]u_t+\frac{D_u}{D_v}uu_t+\frac{(D_u u+D_v v)}{D_v(D_v-D_u)}[D_v(u_t+v_t)-(D_v-D_u)u_t]\,dx\\ &=\int_0^L(v-u_t)u_t+\frac{D_u}{D_v}uu_t-\frac{(D_u u+D_v v)}{D_v}u_t+\frac{(D_u u+D_v v)[D_u u_{xx}+D_v v_{xx}-\varepsilon h_1(v)]}{D_v-D_u}\,dx\\ &=-\int_0^L u_t^2+\frac{(D_u u_x+D_v v_x)^2}{D_v-D_u}+\varepsilon\frac{(D_u u+D_v v)h_1(v)}{D_v-D_u}\,dx\leqslant 0.\end{aligned}$$

In addition, if

$$\frac{d}{dt}\mathcal{L}[u(\cdot,t),v(\cdot,t)]=0\quad(-\infty<t<\infty),$$

then $u_t=D_u u_x+D_v v_x=h_1(v)=0$ holds for all x. We have $v\equiv 0$ by $h_1(v)=0$ and the second condition of Eq. (2.11), and hence $u_t\equiv u_x\equiv 0$. Therefore, it follows from the first

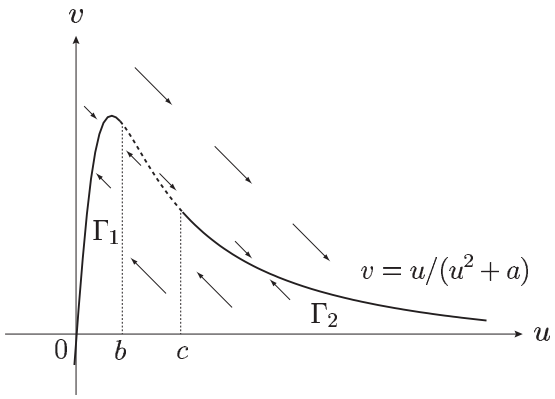

FIG. 1. The flow of Eq. (2.14) on the first quadrant of uv plane. Here, the horizontal and vertical axes indicate u and v, respectively. The equilibria are given by $v = u/(u^2 + a)$. The solid line represents a family of stable equilibria Γ, which is divided into two connected components Γ_1 and Γ_2. On the other hand, the dashed line represents that of unstable equilibria.

equation of Eq. (2.10) that $f_1(u) = 0$, which implies $u \equiv 0$ by the first condition of Eq. (2.11). Thus, we see that $\mathcal{L}(u,v)$ is a Lyapunov function for Eq. (2.10), which proves the global stability of the trivial equilibrium (cf. Ref. [13]).

Remark 1. The functional

$$\mathcal{E}(u,v) := \int_0^L (u+v)\,dx$$

also plays as a Lyapunov function for $\varepsilon > 0$ since the solutions $u(x,t)$ and $v(x,t)$ are nonnegative. The above functional $\mathcal{L}$, however, plays as a Lyapunov function for $\varepsilon = 0$ as well as $\varepsilon > 0$. In fact, when $\varepsilon = 0$, the Lyapunov function $\mathcal{L}$ shows that the flow of our system allows a global attractor in the space with the constraint Eq. (1.2). Such an attractor can be expressed by the union of all the unstable manifolds of equilibria [13] when the attractor has multiequilibria. This dynamical structure, however, is destroyed by a perturbation that breaks the constraint, and it turns to an attractor consisting of only a trivial equilibrium; in our parameter setting, Eq. (2.13) has a unique trivial equilibrium for $\varepsilon > 0$, while it has many equilibria including a single spike under the constraint for $\varepsilon = 0$.

In what follows, we investigate the dynamics of nonnegative solutions of Eq. (2.10) with a specific nonlinearity, Eq. (2.12). First, we consider a system of ODEs,

$$\begin{aligned} u_t &= -\frac{u}{u^2+a} + v \\ v_t &= \frac{u}{u^2+a} - v, \end{aligned} \tag{2.14}$$

which is obtained from Eq. (2.10) with Eq. (2.12) by setting $D_u = D_v = 0$ and $\varepsilon = 0$. In this case, the flow of Eq. (2.14) on the first quadrant is shown in Fig. 1, and the family of stable equilibria Γ is given by

$$\Gamma = \left\{(u,v) | v = \frac{u}{u^2+a},\ \frac{u^2-a}{(u^2+a)^2} < 1\right\}.$$

Moreover, Γ is divided into two connected components given by $\Gamma_1 = \{(u,v)|(u,v) \in \Gamma, u < b\}$ and $\Gamma_2 = \{(u,v)|(u,v) \in \Gamma, u > c\}$, where b and c are defined by

$$\frac{b^2-a}{(b^2+a)^2} = \frac{c^2-a}{(c^2+a)^2} = 1, \quad 0 < \sqrt{a} < b < c. \tag{2.15}$$

Next, we consider the stability of a homogeneous equilibrium $(u^*,v^*) \in \Gamma_2$ in the unperturbed reaction-diffusion system

$$\begin{aligned} u_t &= D_u u_{xx} - \frac{u}{u^2+a} + v \\ v_t &= D_v v_{xx} + \frac{u}{u^2+a} - v. \end{aligned} \tag{2.16}$$

It follows from Eqs. (2.4) and (2.5) that for fixed D_u and D_v with $D_v > D_u$, (u^*,v^*) is stable for

$$\frac{(u^*)^2-a}{[(u^*)^2+a]^2} > \frac{D_v}{D_u},$$

while it is unstable for

$$\frac{(u^*)^2-a}{[(u^*)^2+a]^2} < \frac{D_v}{D_u}. \tag{2.17}$$

Therefore, we see that $(u^*,v^*) \in \Gamma_2$ is unstable if u^* is close to c, because $(c^2-a)/(c^2+a)^2 < D_v/D_u$ holds for all D_u and D_v with $D_v > D_u$ by virtue of Eq. (2.15).

We now numerically investigate the dynamics of nonnegative solutions of

$$\begin{aligned} u_t &= D_u u_{xx} - \frac{u}{u^2+a} + v \\ v_t &= D_v v_{xx} + \frac{u}{u^2+a} - v - \varepsilon v^2 \end{aligned} \quad (0 < x < L), \tag{2.18}$$

under the periodic boundary condition. Our simulations are based on a standard pseudospectral method [14,15], and the numerical scheme is found in the Appendix. The values of parameters are given by

$$a = 0.1, \quad \varepsilon = 0.01, \quad D_u = 0.001, \quad D_v = 0.05, \tag{2.19}$$

with the interval length $L = 2\pi$. In this case, $[c, c/(c^2+a)] \approx (0.79, 1.09)$. Moreover, the initial value $[u_0(x), v_0(x)]$ is given by a small random perturbation on the value (2.0,2.0).

Our simulations show that the dynamics of Eq. (2.18) consists of four stages; the dynamics from the second stage to the fourth stage is shown in Fig. 2 (the dynamics of all stages is provided in a supplemental movie file). On the first stage, the solution moves along the line defined by $u + v = 4$ with $O(1)$ speed, and the dynamics can be given by Eq. (2.3). After the solution approaches Γ_2, it moves along Γ_2 and undergoes the diffusion-driven instability when it enters into a region defined by Eq. (2.17); Γ_2 is a slow manifold that plays the onset of Turing-like patterns, and the dynamics on Γ_2 can be given by Eq. (2.9). On the third stage, the amplitude of the Turing-like patterns becomes large and spatial patterns consisting of some spikes appear. Numerical simulations support that the dynamics on this stage can be approximated by the dynamics of the unperturbed system Eq. (2.16) when ε is sufficiently small. Finally, on the fourth stage, the number of spikes decreases, and the solution eventually converges to the trivial equilibrium; it seems that each spike disappears independently if the distance to the nearest spike is far. The decreasing of spikes can be also observed in the unperturbed system

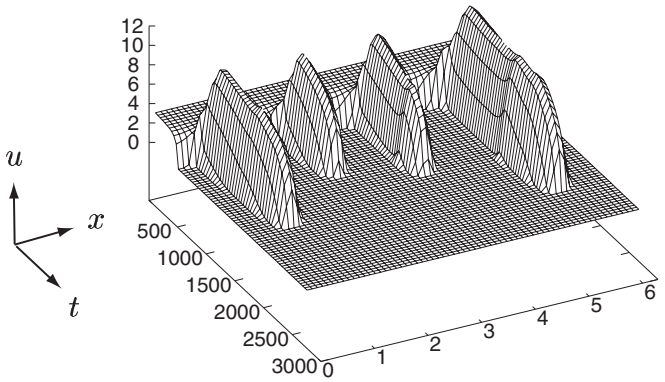

FIG. 2. The dynamics of solutions of Eq. (2.18) after the approach of them to the slow manifold Γ_2. The values of $u(x,t)$ on $0 \leqslant x \leqslant 2\pi$ and $7 \leqslant t \leqslant 2800$ are presented by a 3D graph. In this numerical simulation, the parameter values are given by Eq. (2.19), and the initial value is given by $[2.0+\varepsilon_1(x), 2.0+\varepsilon_2(x)]$, where $\varepsilon_1(x)$ and $\varepsilon_2(x)$ are independent uniform pseudorandom numbers in $[-0.005, 0.005)$ for each $x \in [0,2\pi]$. The profile of $v(x,t)$ is omitted here because the amplitude and spatial variation of $v(x,t)$ for each t are relatively smaller than those of $u(x,t)$. An animation that shows the dynamics of solutions for $0 \leqslant t \leqslant 2800$ is provided in the Supplemental Material [18]. (We recommend that the readers watch the animated movie file of how the spatial pattern is changing; the green and yellow curves represent u and v, respectively. Notice that the time scale on $0 \leqslant t \leqslant 7$ is 16 times as fast as that on $7 \leqslant t \leqslant 2800$.) Finally, we note that the final trivial steady state of the solutions is on the manifold Γ_1 disconnected from Γ_2.

Eq. (2.16) until a single spike remains, and the mathematical justification for the stability of the single spike was shown in Refs. [3,4] (see also Ref. [7]). On the other hand, in the perturbed system, every spike disappears. Moreover, the time scale of the collapse of spikes in Eq. (2.18) is considerably faster than that in Eq. (2.16).

Remark 2. In our numerical simulations, it is difficult to observe the collapse of a single spike if we take sufficiently small ε. A reasonable explanation is that the single spike would be metastable patterns evolving with the speed of $O(e^{-C/\varepsilon})$, which should be investigated in a further study. From a viewpoint of physics, it is desirable to choose the value of ε such that $1/\varepsilon$ considered as the time scale associated to the perturbation terms is much larger than L^2/D_u (=30 000) considered as the typical time for one particle to travel through the system. In our simulation, we choose $\varepsilon = 0.01$ such that the collapse of spikes can be observed within a time interval on which the accuracy of numerical computations can be guaranteed.

Thus, we have shown that a reaction-diffusion model with a globally stable homogeneous equilibrium can exhibit large amplitude Turing-like patterns in the transient dynamics. This example demonstrates that interesting spatiotemporal patterns can be often observed in the transient dynamics of reaction-diffusion systems (cf. Ref. [9]).

Remark 3. The above second stage can be understood by a local center-unstable manifold theory [16,17]. In fact, the unperturbed system allows a center-unstable manifold consisting of the continuum of the homogeneous equilibria parametrized by s and a family of unstable manifolds emanating from the equilibria in the continuum. The perturbed system still has a similar structure for sufficiently small ε.

III. PERTURBATIONS FROM OUTSIDE OF SYSTEMS

In the previous section, we have investigated the effects of perturbations to reaction-diffusion systems with mass conservation; the total mass of the perturbed system is slowly varied by the perturbations generated by interactions between the components within the system. In this section, we investigate the case that the total mass of a system is affected by the outside of the system. Namely, we consider a larger system involving the unperturbed system with a conservation property.

We are concerned with a reaction-diffusion model,

$$\begin{aligned} u_t &= D_u u_{xx} + f(u,v) + \varepsilon g_1(s,w) \\ v_t &= D_v v_{xx} - f(u,v) + \varepsilon g_2(s,w) \quad (0 < x < L) \\ w_t &= \varepsilon h(s,w), \end{aligned} \tag{3.1}$$

under the periodic boundary condition, where $w = w(t)$ and

$$s = s(t) := \frac{1}{L}\int_0^L (u+v)\,dx. \tag{3.2}$$

By adding the first and second equations of Eq. (3.1) and integrating over $[0,L]$, we have

$$\begin{aligned} \dot{s} &= \varepsilon[g_1(s,w) + g_2(s,w)] \\ \dot{w} &= \varepsilon h(s,w), \end{aligned} \tag{3.3}$$

which represents an interaction between the inside and outside of a domain where the unperturbed reaction-diffusion model is defined. We suppose that Eq. (3.3) is a conserved system; there exists a function of $H = H(s,w)$ such that

$$\frac{d}{dt}H[s(t),w(t)] \equiv 0 \tag{3.4}$$

holds for solutions of Eq. (3.3). The most simple examples of g_1, g_2, and h are given by

$$g_1(s,w) \equiv 0, \quad g_2(s,w) = -(w-\alpha), \quad \text{and} \quad h(s,w) = s - \beta, \tag{3.5}$$

respectively, where α and β are constants, and

$$H(s,w) = (w-\alpha)^2 + (s-\beta)^2. \tag{3.6}$$

Equation (3.1) can be considered as a conceptual model describing an interaction between a compartment and a homogeneous medium surrounding the compartment in a larger closed system (see Fig. 3). We assume that the interaction can be observed through the dynamics of the total mass of the components within the compartment.

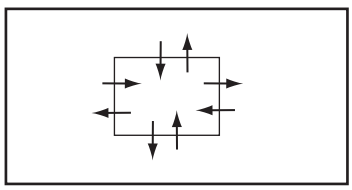

FIG. 3. A compartment and mass flows in a larger closed system.

In what follows, we investigate the dynamics of nonnegative solutions of Eq. (3.1) with a specific nonlinearity,

$$f(u,v) = [(u+a)v - b]u, \tag{3.7}$$

and Eq. (3.5), i.e.,

$$\begin{aligned} u_t &= D_u u_{xx} + [(u+a)v - b]u, \\ v_t &= D_v v_{xx} - [(u+a)v - b]u - \varepsilon(w-\alpha) \quad (0 < x < L), \\ w_t &= \varepsilon\left[\frac{1}{L}\int_0^L (u+v)\,dx - \beta\right] \end{aligned} \tag{3.8}$$

under the periodic boundary condition, where a, b, α, and β are positive constants with $0 < a < \sqrt{b}$. From a viewpoint of mathematical analysis, we note that Eq. (3.8) is a limiting system of

$$\begin{aligned} u_t &= D_u u_{xx} + [(u+a)v - b]u, \\ v_t &= D_v v_{xx} - [(u+a)v - b]u - \varepsilon(w-\alpha) \quad (0 < x < L), \\ w_t &= D_w w_{xx} + \varepsilon(u+v-\beta) \end{aligned}$$

as $D_w \to +\infty$. Although Eq. (3.8) is a three-component model, regarding it as a perturbed system of the two-component system, we can treat Eq. (3.8) in a similar manner to the two-component case in Sec. II.

In order to investigate the dynamics of Eq. (3.8), we consider a system of ODEs,

$$\begin{aligned} u_t &= [(u+a)v - b]u \\ v_t &= -[(u+a)v - b]u, \end{aligned} \tag{3.9}$$

which is obtained from Eq. (3.8) by setting $D_u = D_v = 0$ and $\varepsilon = 0$. We consider nonnegative solutions of Eq. (3.9) because the closure of the first quadrant is an invariant set of Eq. (3.9); the flow of Eq. (3.9) on this set is shown in Fig. 4. The family

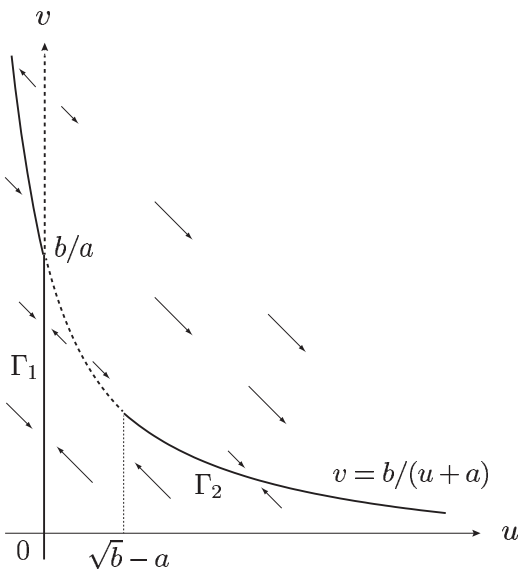

FIG. 4. The flow of Eq. (3.9) on the first quadrant of uv plane. Here, the horizontal and vertical axes indicate u and v, respectively. The equilibria are given by $v = b/(u+a)$ or $u = 0$. The solid line represents a family of stable equilibria Γ, which is divided into two connected components, Γ_1 and Γ_2. On the other hand, the dashed line represents that of unstable equilibria.

of stable equilibria Γ is given by $\Gamma = \Gamma_1 \cup \Gamma_2$, where

$$\Gamma_1 = \left\{(0,\xi) \mid 0 \leqslant \xi < \frac{b}{a}\right\},$$

and

$$\Gamma_2 = \left\{\left(\eta, \frac{b}{\eta+a}\right) \,\middle|\, \eta > \sqrt{b} - a\right\}. \tag{3.10}$$

By adding diffusion terms to Eq. (3.9), we obtain the unperturbed reaction-diffusion system

$$\begin{aligned} u_t &= D_u u_{xx} + [(u+a)v - b]u \\ v_t &= D_v v_{xx} - [(u+a)v - b]u. \end{aligned} \tag{3.11}$$

By using a standard argument based on the maximum principle, it is easily shown that a solution of Eq. (3.11) with a nonnegative initial value takes nonnegative values for all x and $t > 0$.

We consider the stability of a homogeneous equilibrium on Γ in Eq. (3.11). It follows from Eq. (2.4) that $(0,\xi) \in \Gamma_1$ is stable for all positive D_u and D_v. On the other hand, it follows from Eqs. (2.4) and (2.5) that for fixed D_u and D_v with $D_v > D_u$, $[\eta, b/(\eta+a)] \in \Gamma_2$ is stable for

$$\eta > \eta_c,$$

while it is unstable for

$$\sqrt{b} - a < \eta < \eta_c, \tag{3.12}$$

where

$$\eta_c := \sqrt{\frac{D_v b}{D_u}} - a. \tag{3.13}$$

Thus, we see that Eq. (3.11) has a similar structure to the two-component model Eq. (2.16) in Sec. II.

Now let us consider Eq. (3.8). Equation (3.8) has a family of spatially homogeneous periodic orbits. In fact, when $D_u = D_v = 0$, Eq. (3.8) is reduced to an ODE system,

$$\begin{aligned} \dot{u} &= [(u+a)v - b]u \\ \dot{v} &= -[(u+a)v - b]u - \varepsilon(w-\alpha). \\ \dot{w} &= \varepsilon(u+v-\beta) \end{aligned} \tag{3.14}$$

By adding the first and second equations of Eq. (3.14), we have

$$\begin{aligned} \dot{s} &= -\varepsilon(w-\alpha) \\ \dot{w} &= \varepsilon(s-\beta), \end{aligned} \tag{3.15}$$

where $s = u + v$. Notice that Eq. (3.15) is the same as Eq. (3.3) with Eq. (3.5). Since solutions of Eq. (3.15) in the (s,w) plane consist of a family of circles with the center (β,α), Eq. (3.8) has a homogeneous periodic orbit, say C, whose (u,v) components slowly oscillate on Γ_2 given by Eq. (3.10).

Noting that Γ_2 can be regarded as a slow manifold that plays the onset of Turing-like patterns in a similar manner as stated in Sec. II, we investigate how the homogeneous periodic orbit C changes as the value of D_v increases in Eq. (3.8). In the same way as Sec. II, we numerically solve Eq. (3.8) for various values of D_v under the parameter values

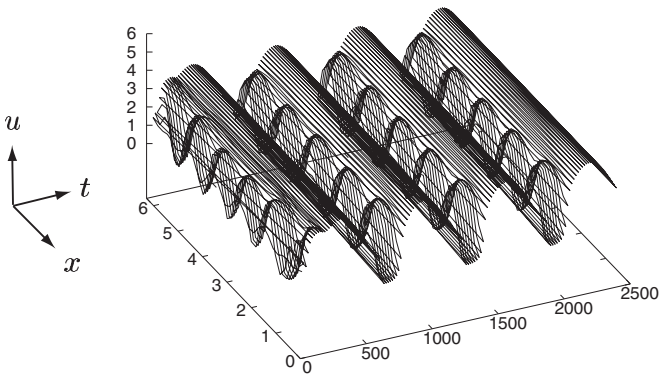

FIG. 5. An alternating repetition of (almost) homogeneous oscillations and large amplitude Turing-like patterns in the dynamics of Eq. (3.8). The values of $u(x,t)$ on $0 \leqslant x \leqslant 2\pi$ and $0 \leqslant t \leqslant 2400$ are presented by a 3D graph. In this numerical simulation, $D_v = 0.03$ and the parameter values are given by Eq. (3.16). Moreover, the initial values are given by $[u_0(x), v_0(x)] = [1.5 + \varepsilon_1(x), 1.6 + \varepsilon_2(x)]$ and by $w_0 = 2.5$, where $\varepsilon_1(x)$ and $\varepsilon_2(x)$ are independent uniform pseudorandom numbers in $[-0.005, 0.005)$ for each $x \in [0, 2\pi]$. The profile of $v(x,t)$ is omitted here because the amplitude and spatial variation of $v(x,t)$ for each t are relatively small than those of $u(x,t)$. An animation that shows the dynamics of u, v, and s for $0 \leqslant t \leqslant 2400$ is provided in the Supplemental Material [18]. (We recommend that the readers watch the animated movie file of how the spatial pattern is changing; the green, blue, and red curves represent u, v, and s, respectively).

given by

$$a = 1.0, \quad b = 4.0, \quad \alpha = 2.5,$$
$$\beta = 4.0, \quad \varepsilon = 0.01, \quad D_u = 0.01. \tag{3.16}$$

The initial values $[u_0(x), v_0(x)]$ and w_0 are given by a small random perturbation on the value $(1.5, 1.6) \in \Gamma_2$ and by $w_0 = 2.5$, respectively. Notice that the small random perturbation is an indispensable factor in nonhomogeneous spatial pattern formation; the solution without small random perturbations uniformly oscillates for any D_v. Moreover, for relatively small D_v/D_u, the solution with an initial small random perturbation does not exhibit nonhomogeneous spatial patterns. This is supported by our numerical simulations for $D_v \lesssim 0.026$. These features and the results presented below can also be obtained near the above specific parameters and initial values.

Figure 5 shows an alternating repetition of spatially (almost) homogeneous oscillations and large amplitude Turing-like patterns for $D_v = 0.03$, which is induced by the destabilization effect of the diffusion terms on the homogeneous periodic orbit C. In this case, we have chosen the initial values so as to satisfy $u_0(x) < \eta_c \approx 2.46$, where η_c is given by Eq. (3.13); if this condition is not satisfied, such an alternating repetition is not necessarily observed. In fact, the spatial fluctuation of a solution with a small random initial disturbance vanishes before the solution moving along Γ_2 enters a region defined by Eq. (3.12), and hence its dynamics can be reduced to the dynamics of Eq. (3.14).

It should be emphasized that Eq. (3.4) plays a central role for generating the above alternating repetition. In general reaction-diffusion systems, if a solution with an initial value near a homogeneous periodic orbit approaches a stable Turing pattern for appropriate values of diffusion coefficients, then the solution cannot leave the stable Turing pattern. On the other hand, in our reaction-diffusion system Eq. (3.8), a solution with an initial value near the homogeneous periodic orbit C can leave the Turing-like patterns because of the constraint Eq. (3.4) with Eq. (3.6). In fact, Turing-like patterns are not stable stationary solutions. Moreover, as explained in Sec. II, the solution exhibits Turing-like patterns when the value of s decreases and approaches its minimum value, i.e., the solution moving along Γ_2 enters a region defined by Eq. (3.12). Thereafter, by the constraint Eq. (3.4) with Eq. (3.6), the value of s must increase and move away from its minimum value. Then, the solution is far away from the region defined by Eq. (3.12) and its spatial profile becomes flat. Consequently, the solution returns to a neighborhood of the homogeneous periodic orbit C when the value of s approaches its maximum value.

Remark 4. Suppose that a homogeneous equilibrium of a reaction-diffusion system undergoes Turing instability and the amplitude of bifurcating patterns becomes large for appropriate values of the diffusion coefficients. We periodically and slowly vary a parameter included in the reaction terms around a critical value at which the stability of the homogeneous equilibrium changes.[1] Then, it might be possible to observe an alternating repetition of spatially (almost) homogeneous oscillations and large amplitude Turing-like patterns. However, in general, such an alternating repetition cannot be observed; only either spatially homogeneous oscillations or Turing-like patterns can be observed. This fact suggests that some sort of mechanism allowing solutions to leave Turing-like patterns and to return to homogeneous oscillatory states are underlying in generating an alternating repetition of spatially (almost) homogeneous oscillations and large amplitude Turing-like patterns.

IV. CONCLUDING REMARKS

In this study, we have investigated spatiotemporal dynamics obtained by small perturbations to reaction-diffusion systems with mass conservation. First, we have shown that a reaction-diffusion model with a globally stable homogeneous equilibrium can exhibit large amplitude Turing-like patterns in the transient dynamics. This model has a Lyapunov function, and hence any solution converges to the homogeneous equilibrium. On the other hand, the model has a slow manifold, which is the onset of Turing-like patterns, and hence solutions passing through a neighborhood of the slow manifold can generate Turing-like patterns.

Next, we have proposed a three-component reaction-diffusion model that exhibits an alternating repetition of spatially (almost) homogeneous oscillations and large amplitude Turing-like patterns. This model has a homogeneous periodic

[1] In this case, the (in)stability is determined by the behavior of eigenvalues of the linearized operator at the homogeneous equilibrium for each fixed value of the parameter to be periodically varied. This instability should not be called Turing instability because the values of the diffusion coefficients are fixed.

orbit moving along a slow manifold, which includes the onset of Turing-like patterns, and hence a solution with an initial value near the periodic orbit can approach Turing-like patterns. On the other hand, the model has another conservation that is different from the total mass of the components of unperturbed reaction-diffusion system. Therefore, the solution can leave Turing-like patterns by virtue of this conservation. Consequently, the solution can return to a neighborhood of the homogeneous periodic orbit.

Although our models were proposed for studying mathematical aspects of perturbations to reaction-diffusion systems with mass conservation, our motivation of this study originates from a biological issue concerning cell polarization; spatially distinctive accumulation of signaling molecules is established inside the cell. A certain class of reaction-diffusion systems with mass conservation were proposed as a conceptual model to explain cell polarization under the assumption that the masses of molecules are constant during the polarization. Therefore, our approach could be useful to study cell polarization under the situation that the masses of molecules are slowly varied through various slow events such as gene expression and protein synthesis.

Our approach provides a viewpoint for studying the effects of perturbations on the dynamics of reaction-diffusion systems with mass conservation. At present, this work is a first step, which should be developed to a theory for analyzing of perturbed reaction-diffusion systems with mass conservation.

ACKNOWLEDGMENTS

The authors thank the referees for their useful suggestions and comments, which were helpful in improving the original manuscript. The authors were supported in part by the Grant-in-Aid for Exploratory Research, Grant No. 24654044, JSPS. The second author was also partially supported by the Grand-in-Aid for Scientific Research(B), Grant No. 26287025, JSPS.

APPENDIX: NUMERICAL SCHEME

Applying the Fourier transformation, a reaction-diffusion system in the real space,

$$u_t = Du_{xx} + f(u), \tag{A1}$$

can be converted to a system of ODEs in the Fourier space,

$$\frac{d\hat{u}_k}{dt} = -Dk^2\hat{u}_k + f_k(\hat{u}), \tag{A2}$$

where k denotes the wavenumber, and

$$f_k(\hat{u}) = [\widehat{f(u)}]_k = \{\mathcal{F}[f(\mathcal{F}^{-1}\hat{u})]\}_k,$$

with the Fourier transformation $\mathcal{F}$ and its inverse $\mathcal{F}^{-1}$. In simple terms, the pseudospectral method for numerically solving Eq. (A1) on $(-L/2, L/2)$ under the periodic boundary condition is a numerical scheme to solve Eq. (A2) by using the Runge-Kutta method under the condition that the amplitudes of high-frequency Fourier modes $e^{2\pi ikx/L}$ vanish; $\hat{u}_k = 0$ ($k \in \mathbf{Z}$, $|k| \geqslant N/2$), where $N = 2^m$ ($m \in \mathbf{N}$) is the total number of Fourier modes in the numerical computation (finite dimensional approximation) with the aid of FFT.

Let $v_k = \hat{u}_k \exp(-Dk^2t)$. Then, we have

$$\frac{dv_k}{dt} = f_k(\hat{u})\exp(Dk^2t) := G_k(v,t). \tag{A3}$$

Applying the fourth-order Runge-Kutta scheme to Eq. (A3), we have

$$\begin{aligned}
v_k(t+\Delta t) &= v_k(t) + (h_1 + 2h_2 + 2h_3 + h_4)\Delta t/6,\\
h_1 &= G_k(v,t) = f_k(\hat{u})\exp(Dk^2t),\\
\hat{u}_1' &= \{\hat{u}_k(t) + h_1\exp(-Dk^2t)\Delta t/2\}\exp(-Dk^2\Delta t/2),\\
h_2 &= G_k(v + h_1\Delta t/2, t + \Delta t/2)\\
&= f_k(\hat{u}_1')\exp[(Dk^2(t+\Delta t/2))],\\
\hat{u}_2' &= \{\hat{u}_k(t) + h_2\exp(-Dk^2t)\Delta t/2\}\exp(-Dk^2\Delta t/2),\\
h_3 &= G_k(v + h_2\Delta t/2, t + \Delta t/2)\\
&= f_k(\hat{u}_2')\exp[Dk^2(t+\Delta t/2)],\\
\hat{u}_3' &= \{\hat{u}_k(t) + h_3\exp(-Dk^2t)\Delta t\}\exp(-Dk^2\Delta t),\\
h_4 &= G_k(v + h_3\Delta t, t + \Delta t)\\
&= f_k(\hat{u}_3')\exp[Dk^2(t+\Delta t)].
\end{aligned}$$

Thus, we obtain the following numerical scheme for Eq. (A2):

$$\begin{aligned}
\hat{u}_k(t+\Delta t) = \hat{u}_k(t)\exp(-Dk^2\Delta t) &+ \{h_1'\exp(-Dk^2\Delta t)\\
&+ 2(h_2' + h_3')\exp(-Dk^2\Delta t/2) + h_4'\}\Delta t/6,
\end{aligned}$$

where

$$h_1' = f_k(\hat{u}), \quad h_2' = f_k(\hat{u}_1'), \quad h_3' = f_k(\hat{u}_2'), \quad h_4' = f_k(\hat{u}_3').$$

It should be noted that this scheme can be applicable to Eq. (3.8) because the integration term in Eq. (3.8) corresponds to the sum of the amplitudes of the zero Fourier mode ($k = 0$) for u and v in Eq. (3.8). Although numerical schemes to solve PDEs by using the pseudospectral method are rather more involved than standard finite difference schemes, they can give precise numerical results even if the PDEs satisfy (infinitely many) conservation laws such as the KdV equation [14,15].

[1] M. Otsuji, S. Ishihara, C. Co, K. Kaibuchi, A. Mochizuki, and S. Kuroda, PLoS Comp. Biol. **3**, e108 (2007).
[2] S. Ishihara, M. Otsuji, and A. Mochizuki, Phys. Rev. E **75**, 015203 (2007).
[3] Y. Morita and T. Ogawa, Nonlinearity **23**, 1387 (2010).
[4] Y. Morita, J. Appl. Anal. Comp. **2**, 57 (2012).
[5] S. Jimbo and Y. Morita, J. Diff. Eqs. **255**, 1657 (2013).
[6] T. Okuda Sakamoto, Nonlinearity **26**, 2027 (2013).
[7] E. Latos and T. Suzuki, J. Math. Anal. Appl. **411**, 107 (2014).
[8] J. E. Pearson, Science **216**, 189 (1993).
[9] Y. Nishiura, *Far-from-Equilibrium Dynamics, Translations of Mathematical Monographs* (American Mathematical Society, Providence, RI, 2002), Vol. 209.
[10] J. D. Murray, *Mathematical Biology*, 2nd ed. (Springer-Verlag, New York, 1989).

[11] S. H. Strogatz, *Nonlinear Dynamics and Chaos* (Westview Press, Boulder, CO, 2000).

[12] D. Henry, *Geometric Theory of Semilinear Parabolic Equations* (Springer-Verlag, Berlin/New York, 1981).

[13] J. K. Hale, *Asymptotic Behavior of Dissipative Systems, Mathematical Surveys and Monographs*, Vol. 25 (American Mathematical Society, Providence, RI, 1988).

[14] D. Gottlieb and S. A. Orszag, *Numerical Analysis of Spectral Methods: Theory and Applications*, CBMS-NSF Regional Conference Series in Applied Mathematics (SIAM, Philadelphia, 1977), Vol. 26.

[15] B. Fornberg, *A Practical Guide to Pseudospectral Methods* (Cambridge University Press, Cambridge, 1995).

[16] P. W. Bates, K. Lu, and C. Zeng, *Existence and Persistence of Invariant Manifolds for Semiflows in Banach Space* (American Mathematical Society, Providence, RI, 1998), Vol. 135.

[17] P. W. Bates, K. Lu, and C. Zeng, Trans. Am. Math. Soc. **352**, 4641 (2000).

[18] See Supplemental Material at http://link.aps.org/supplemental/10.1103/PhysRevE.92.012908 for the animation corresponding to Figs. 2 and 5.